An economically feasible optimization of photovoltaic provision using real electricity demand: A case study in New York city

Rui Zhu [a], Man Sing Wong [a,*], Mei-Po Kwan [b], Min Chen [c,d,e], Paolo Santi [f,g], Carlo Ratti [f]

[a] *Department of Land Surveying and Geo-Informatics, The Hong Kong Polytechnic University, Hong Kong, China*
[b] *Department of Geography and Resource Management, The Chinese University of Hong Kong, Hong Kong, China*
[c] *Key Laboratory of Virtual Geographic Environment (Ministry of Education of PR China), Nanjing Normal University, Nanjing, 210023, China*
[d] *State Key Laboratory Cultivation Base of Geographical Environment Evolution (Jiangsu Province), Nanjing, 210023, China*
[e] *Jiangsu Center for Collaborative Innovation in Geographical Information Resource Development and Application, Nanjing, 210023, China*
[f] *Senseable City Laboratory, Department of Urban Studies and Planning, Massachusetts Institute of Technology, Cambridge MA 02139, USA*
[g] *Istituto di Informatica e Telematica del CNR, 56124 Pisa, Italy*

ARTICLE INFO

ABSTRACT

Solar farming has been experiencing explosive development in recent years. However, developing solar farming in urban areas is challenged by the heterogeneous distribution of solar irradiation in spatial and degradation of photovoltaic (PV) efficiency that make the economic performance uncertain. To tackle this problem, this study develops a spatio-temporal analytic model and a techno-economic assessment model to optimize PV provision to ensure that a PV system can meet the electricity demand and obtain reasonable profit simultaneously. Specifically, based on the estimation of solar potential on three-dimensional urban envelopes, the study determines PV favorable locations that are quantitatively large and spatially concentrated. Then, PV capacities in two comparative architectures, i.e., *self-reliance* relying on own building surfaces and *external-support* seeking supports from external rooftops, are planned to meet real electricity demand. Furthermore, the PV capacity is optimized, constrained by a constant electricity rate without Feed-in Tariff, a decreasing PV efficiency, and an increasing cost for maintenance. A case study in New York City suggests that the optimized PV installation can significantly offset household electricity consumption. In addition, the estimated net profit is significant even in rigorous conditions, which is inspiring for promoting distributed solar harvesting and competing with the local electricity market.

1. Introduction

Cities consumed around 70% of global energy (Creutzig et al., 2015) that contributes to urban heat islands (Zhu, Guilbert et al., 2017, 2020; Zhu, Wong et al., 2017), produces enormous carbon emissions (Lin & Li, 2020; Zhou et al., 2021), and exacerbates air pollution (Kan et al., 2020). Thus, it is imperative to promote renewable energy to develop energy-efficient cities (Masson et al., 2014). As one of the most tremendous energy sources that are available in every corner of the earth, solar energy has been increasingly used in recent years to generate electricity (Chu & Majumdar, 2012; Ma et al., 2017; Molina et al., 2017) and provide heating and cooling services (Kalder et al., 2018; Li et al., 2020, 2015).

In recent years, photovoltaics have been widely used by companies and individuals to harvest solar energy (Meyers et al., 2018; Wolske et al., 2018). Distributed solar PV generation in cities takes advantage of solar favorable and free space to power local communities by establishing local utility smart grid (Baum et al., 2019), as opposed to utility-scale solar PV plants that are usually located at remote and bare land (e.g., the desert in California, the U.S.) to provide a stable and large amount of electricity. The grid enables the construction of an adaptive solar PV system to serve real-time electricity demand, reduce the loss of electric power due to long-distance transmission, and improve the resilience of the national grid. To make this architecture efficient, an optimization with three hierarchical stages is needed: (i) an accurate estimation of annual solar potential considering the effects of urban morphology, (ii) an adaptive solar PV plan that meets real electricity demand, and (iii) a reliable economic assessment to ensure that the planned distributed system can benchmark or compete with the current electricity rate.

Many studies have developed various models to estimate spatial distribution of solar irradiation accurately, which either focused on

---

rooftops (Calcabrini et al., 2019; Jakubiec & Reinhart, 2013; Li et al., 2016; Wong et al., 2016; Zhong, Zhang, Chen, Zhang et al., 2021), façades (Catita et al., 2014; Liang et al., 2014, 2015; Redweik et al., 2013; Zhong, Zhang, Chen, Wang et al., 2021), or all the three partitions including ground (Erdélyi et al., 2014; Hofierka & Zlocha, 2012; Lindberg et al., 2015; Lobaccaro et al., 2017; Zhu, Wong et al., 2020; Zhu et al., 2019). Since this study aims to harvest solar energy on building surfaces, the models (Zhu, Wong et al., 2020; Zhu et al., 2019) that estimate shadow effects of buildings on 3D urban envelopes and accumulate solar potential throughout a year are appropriate to compute solar PV potential accurately.

To build an adaptive solar PV system, researchers have noticed the mismatch between demand and supply because of seasonal variations of solar potential and hourly and monthly changes of electricity demand (Richardson & Harvey, 2015; Staffell & Pfenninger, 2018; Ullah et al., 2018), which motivates researchers to propose strategies to improve the resilience, such as optimizing the orientation of PV modules, combining dispersed arrays, and utilizing storage systems (Staffell & Pfenninger, 2018). In the other aspect, a few studies focused on a regional or national level for PV optimization (Park & Lappas, 2017; Renken et al., 2018). However, these studies have not considered the constraint of heterogeneous distribution of solar irradiation at a fine scale of the urban environment. Thus, the first objective of this study is to optimize an executable PV plan based on a given built environment, which needs to maximize the generation of electricity and minimize the occupation of urban surfaces to save the purchasing, installing, and maintaining cost.

It is also crucial to observe that a distributed solar PV system may not be able to benchmark or compete with the local electricity price, although the system can meet electricity demand with a maximized solar capacity and minimized PV size. To address this economic feasibility issue, many studies incorporated electric supply and demand with a life cycle economic assessment (Cristea et al., 2020; Kettani & Bandelier, 2020; Nyholm et al., 2017; Oh et al., 2018; Ren et al., 2020), which usually considers a number of key economic aspects, such as the investment payback period and life cycle cost. However, these studies assumed that the spatial distribution of solar irradiation was homogeneous. In this case, uncertainty remains as the payback period may be substantially longer or the total cost may be more than the local electric price. As a result, the second objective of this study is to construct an economically feasible PV system that can benchmark local electricity prices.

The rest of the paper is organized as follows. Section 2 reviews the literature on solar potential estimation, solar urban planning, and solar economic assessment. To optimize PV provision in urban areas, Section 3 proposes a spatio-temporal analytic model to optimize PV size and location and refines a techno-economic assessment model to adjust solar PV capacity to be harvested. Furthermore, as a case study in New York City, Section 4 and Section 5 optimize the solar PV capacity to supply real electricity demand and obtain a reasonable payback period and net profit. Finally, Section 5 presents the discussion and conclusion.

2. Literature review

2.1. Solar potential estimation

Previous studies on estimating solar potential can be organized into three categories: changes of solar distribution on building surfaces across both spatial and temporal domains (Catita et al., 2014; Lindberg et al., 2015; Lobaccaro et al., 2017; Peronato et al., 2018); transformation of solar accessibility when cities are reformed, such as constructing a cluster of new buildings (Zhu et al., 2019); and solar optimization by designing new urban forms or hybrid systems (Bianchi et al., 2014; Zhang et al., 2019). Studies relying on existing buildings to estimate solar irradiation has achieved fine spatial resolution (Catita et al., 2014; Jakubiec & Reinhart, 2013; Zhu, Wong et al., 2020; Zhu et al.,

2019) and varying temporal resolution in seasonal, monthly, or hourly scales (Catita et al., 2014; Jakubiec & Reinhart, 2013; Lindberg et al., 2015; Lobaccaro et al., 2017), which allows an accurate estimation of the spatial distribution of solar irradiation in a built environment. Specifically, the model developed by Zhu, Wong et al. (2020) can estimate the spatial distribution of solar irradiation accurately on 3D urban envelopes that considers the shading effect on rooftops, façades, and ground from surrounding buildings with complex geometries, such as rooftops are concave polygons or rooftops are nested with each other. This satisfies the demand of this study to estimate solar PV potential in a complex urban environment. Also, the model allows users to define spatial and temporal resolution, which makes it possible to propose an executable PV plan with determined size and detailed location by adapting real electricity demand from customers. Therefore, this can address the uncertainty on determining solar PV capacity to be harvested.

2.2. Solar PV planning

An effective way to plan solar PV capacity to be harvested is investigating the interaction between the utility side and demand side to address demands in different scenarios, such as predicted demand in the future (Park & Lappas, 2017; Staffell & Pfenninger, 2018), real-time demand represented by smart meter data (Dyson et al., 2014), and peak demand during the daytime peak hours (Rauf et al., 2020). These studies revealed general characteristics that supply mismatched demand in different spatio-temporal domains, e.g., solar PV potential cannot satisfy instant peak demand during daytime or solar PV potential is quite low during winter that can only meet a small proportion of the demand. Thus, to reveal the largest PV capacity constraint by a minimal occupation of urban surfaces, it is crucial to explicitly reveal solar concentration patterns with high spatio-temporal granularity. One study has demonstrated an estimation of solar energy at a fine spatio-temporal resolution focusing on a large geographical extent of the Arabian Peninsula (Dasari et al., 2019). However, the method introduced in this study is inappropriate for cities, which need a fine scale analysis to plan PV locations. Therefore, the first innovation of this study is proposing a spatio-temporal analytic method to reveal annual solar concentration patterns on different partitions of a built environment, which will be integrated into a framework to optimize the locations of solar PV modules.

There are many ways to optimize the installation of solar PV modules, including identifying optimal orientation and inclination (Dike et al., 2012; Richardson & Harvey, 2015), proposing distributed sites (Lim et al., 2020; Richardson & Harvey, 2015), and developing battery storage (Lim et al., 2020; Park & Lappas, 2017; Richardson & Harvey, 2015). In comparison, our study will propose a new strategy for optimizing distributed sites, with an objective function of maximizing solar farming and minimizing occupied urban surfaces to partly or even entirely meet monthly electricity demand. To solve the installation optimization problem in fine spatial granularity, a possible solution is to investigate the distribution of solar PV capacities affiliated by the corresponding PV areas when a series of designated solar PV intensities are utilized. As few studies have incorporated real electric consumption into spatial optimization of PV modules, the second innovation of our study is demonstrating planning of PV modules from a GIS-based spatio-temporal optimization perspective, with two alternative strategies either utilizing rooftops only or combining the usages of rooftops and façades. In addition, this study will model atmospheric effects and geometrical effects from quantitative and spatial distribution perspectives to achieve an accurate estimation of annual solar PV potential.

2.3. Solar economic assessment

It was suggested that photovoltaics can be utilized better than solar thermal plants to meet local electricity demand when taking costs into consideration (Meyers et al., 2018). By conducting a cost–benefit analysis that estimated cost savings based on the current electricity rate without any subsidy, one study suggested that the proposed system was still economically feasible (Baum et al., 2019). This finding allows us to expect an increasing development of the solar industry when a solar PV system can compete with the current electric price without subsidy. Many countries have also established feed-in tariffs (FiTs) initiatives to promote solar PV modules to generate green electricity, such as Australia (Poruschi & Ambrey, 2019). However, it was found that a higher density of buildings mitigated this promotion trend. Thus, our study will propose optimization based on a benchmark or competitive electricity price without FiTs to facilitate the development of the distributed PV system.

According to the techno-economic assessment (Kettani & Bandelier, 2020; Oh et al., 2018), the installation cost and the consequent operation and maintenance (O&M) cost affect the economic performance of distributed PV systems significantly. To obtain a reliable assessment, the National Renewable Energy Laboratory (NREL) considered that installation cost included the standard cost, labor cost, transformers, sales and marketing, re-roofing, etc., and O&M costs contained several categories, including inverter replacement, operations administration, module replacement, system inspection and monitoring, etc. (Feldman et al., 2021). The other study modeled the investment payback period and life cycle cost that incorporated several parameters, including profits from solar PV generation, capital cost of the PV system, labor cost, annual O&M costs, and tax credit and rebate (Ren et al., 2020). To obtain an executable plan, our study will integrate the constant installation cost and the varying O&M costs into the optimization of PV capacity and PV location to achieve a reasonable payback period. Since PV efficiency decreases gradually (Chandel et al., 2015; Forniés et al., 2021; Ishii & Masuda, 2017), our study will also estimate generated electricity that is changing over the entire life cycle, which will influence the payback period and net profit considerably. One of the most similar studies also used GIS techniques for economic assessment (Mangiante et al., 2020), which only focused on rooftops. In comparison, this study is innovative in three aspects: (i) proposing PV planning on both rooftops and façades simultaneously, (ii) optimizing PV area and location with the maximization of electricity generation and the minimization of the total PV area, and (iii) developing spatial-aware techno-economic assessment to ensure that the planned PV system can obtain reasonable net profit over the life cycle with four strict scenarios, including a continuous increase of maintenance cost, continuous PV degradation, constant electricity price, and direct competition with the market without FiT.

3. Optimization of PV installation

To optimize the deployment of PV modules, our study firstly computes the distribution of annual solar irradiation on 3D urban envelopes based on historical weather data and 3D building data (Fig. 1). Then, this study proposes a spatio-temporal analysis to reveal spatial and quantitative distribution patterns of solar PV capacity, which will be used as a guideline to optimize the strategy of using different urban partitions. Next, the study optimizes solar PV capacity to be harvested based on real electricity consumption. Furthermore, an economic feasibility assessment model is proposed to determine the required solar PV capacity based on the electricity rate and PV installation and O&M costs during the whole life cycle. Simultaneously, a reasonable payback period and net profit are estimated. Important notations for modeling the spatial distribution of solar irradiation and estimating economic feasibility are listed in Table 1.

Table 1
The list of notations for modeling 3D solar irradiation and estimating economic feasibility.

No.	Abbre.	Meaning
1	$\mathcal{P}$	3D polygons as urban envelopes
2	$\mathcal{R}$	3D polygons as rooftops
3	$\mathcal{F}$	3D polygons as façades
4	$\mathcal{G}$	3D polygons as the ground
5	$\mathcal{X}$	3D vectors as ray of light
6	$\mathcal{O}$	3D point clouds
7	S'	3D shadow surfaces by façades without modification
8	S	3D shadow surfaces modified by surrounding buildings
9	e_i	PV intensity – generated electricity at a unit area and a unit period
10	e_p	PV potential – accumulation of e_i for an area and period
11	e_c	PV capacity – accumulation of e_i for an area and period when $e_i \geqslant e_{min}$
12	$p(e)$	The proportion of e_c subject to e_p
13	$p(a)$	The proportion of the area corresponding to $p(e)$
14	u	Solar irradiation on an urban surface
15	r_d	PV degradation rate
16	ε^*	PV transition efficiency for t years
17	c_m^*	The total operational and maintenance cost for t years
18	c_p	The total profit for t years

3.1. Modeling solar PV potential on 3D urban envelopes

Estimation of solar PV potential is based on a 3D solar irradiation distribution model that can accurately estimate the 3D shadow effect between buildings (Zhu, Wong et al., 2020). As footprints of buildings with the height attribute are stored as polygons that can be decomposed into a series of line segments, façades can be built as a group of vertical rectangles so that the vertical edges of each rectangle are with the same height of the building. In addition, each building has a horizontal rooftop with the same geometrical shape of the footprint. Thus, a set of 3D polygons denoted by $\mathcal{P}$ can be used to represent 3D urban envelopes organized by rooftops $\mathcal{R}$, façades $\mathcal{F}$, and ground $\mathcal{G}$, i.e., $\mathcal{P} = \{\mathcal{R}, \mathcal{F}, \mathcal{G}\}$. Furthermore, each 3D polygon p belonging to $\mathcal{P}$ is discretized by spatial homogeneous and contiguous grid cells with a constant resolution so that 3D point clouds denoted by $\mathcal{O}$ can be obtained at the center of the grid cells, which can also be used to present 3D urban envelopes. In particular, for each 3D point o, it is recorded by an unique ID i, a 3D coordinate l on a surface p, and an accumulated solar irradiation u, i.e., $o = \langle i, l, p, u \rangle$.

Then, the model defines each ray of light as a tuple $x = \langle v, z, t, l, u' \rangle$, meaning that the light with solar irradiation u' travels at an elevation v and an azimuth z and arrives on an urban surface at location l and time t. Thus, a complete set of light rays is characterized by 3D vectors and represented by $\mathcal{X}$, which passes through the atmosphere and arrives at the 3D point clouds $\mathcal{O}$. Next, $\mathcal{X}$ can intersect with $\mathcal{R}$ and $\mathcal{F}$, resulting in a collection of 3D shadow surfaces represented by S', which are further updated as S in consideration of the following three scenarios: (i) there is no shadow surface behind a solar-facing façade, (ii) façades already in shadow cannot make shadow surfaces, and (iii) façades with concave rooftops may produce irregular shadow surfaces. Specifically, when a shadow surface intersects façades of the same building because of the concave rooftop, the shadow surface will be cut by the intersected façades so that areas out of the building footprint polygon can be maintained as a modified 3D shadow surface. Note that u on urban envelopes differs from u' of a beam of light because the intersection between $\mathcal{X}$ and $\mathcal{P}$ is not orthogonal most of the time. Therefore, u is transformed from u' based on the energy conservation law. Ultimately, for each 3D point o, u equals 0 when o is below S and u equals $f(u')$ when o is above S.

Based on time t and the city's coordinate l, the Sun Earth Tool was used to compute the elevation angle e and azimuth z needed to compute solar irradiation u' (Sun Earth Tools, 2021). Because cloud cover is one of the most important factors that determine near-ground direct and diffuse solar irradiation u', hourly cloud-cover data has been collected for five years between 2016 and 2020 from World
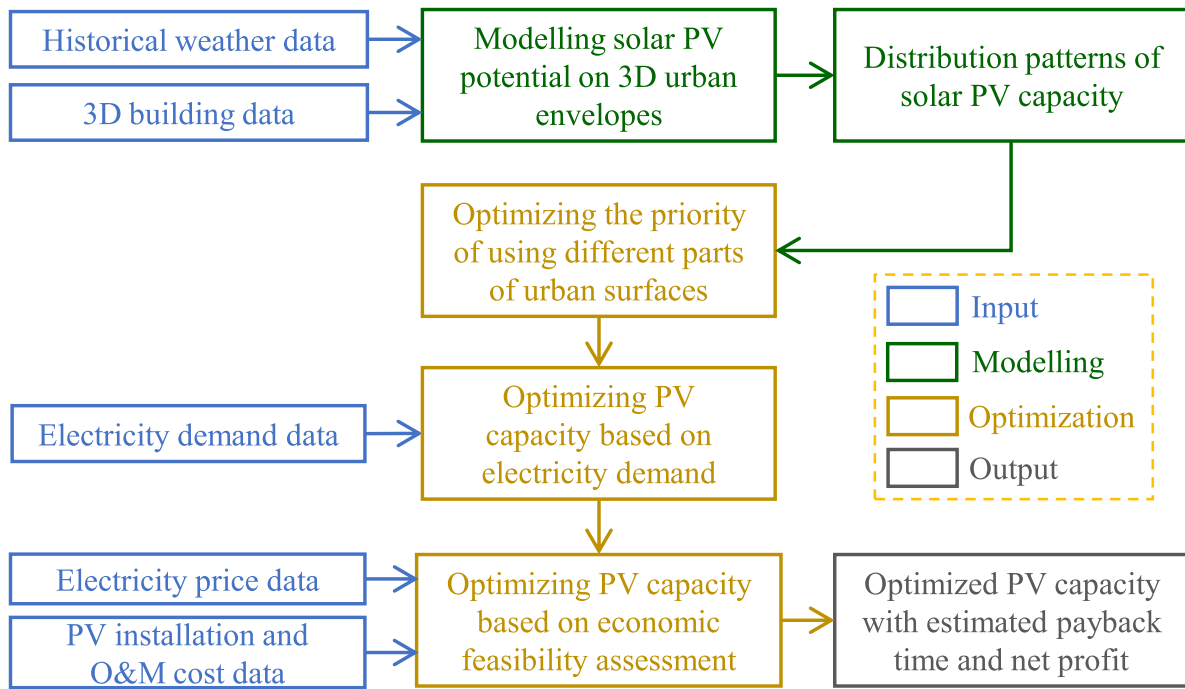
Fig. 1. Flow chat of the optimization framework.

Weather Online (2021), which were used to compute transmittivity α and diffuse proportion β (Huang et al., 2008) that have a historically statistical implication and thus address the uncertainty of unstable weather. The influence of terrain variation on the spatial distribution of solar irradiation is ignored in the study as the study area is flat. With a determined $\langle v, z, \alpha, \beta, l, t \rangle$, the irradiation u on a horizontal urban surface was computed by using Points Solar Radiation in ArcGIS Pro (2021).

3.2. Distribution patterns of solar PV capacity

For a clear presentation, this study defines that *solar PV intensity* denoted by e_i is the electricity generated from a solar PV module with a photovoltaic transition efficiency of ε at a unit area (e.g., 1 m^2) and a unit period (e.g., one second or one day) when solar irradiation is u (Eq. (1)). This study also defines that *solar PV potential* represented by e_p is the accumulation of e_i over a certain area and period (Eq. (2)). For solar farming, it is reasonable to harvest e_p when e_i is quantitatively large. In other words, people prefer harvesting solar energy with a *solar PV capacity* denoted by e_c, where e_{min} is the minimum PV intensity to be harvested (Eq. (3)). Thus, there is a trade-off between solar PV capacity and solar PV intensity, which means that there is only a small amount of solar PV capacity if people desire to harvest high solar PV intensity over a small area of urban surfaces.

$$e_i = \varepsilon \cdot u \tag{1}$$

$$e_p = \int_0^t \int_0^a e_i \tag{2}$$

$$e_c = \int_0^t \int_0^a e_i \mid e_i \geqslant e_{min} \tag{3}$$

It is imperative to reveal distribution patterns of solar PV capacity and the corresponding PV size subject to solar PV intensity to be harvested for proposing practical solar PV planning. If the largest solar PV intensity on an urban partition (e.g., rooftops, façades, or ground) is e_{max}, then the lowest solar PV intensity to be used can be determined as $e_{min} = \delta \cdot e_{max}$, where δ is a relative index between 0 and 1. Given that the total solar PV potential during a period of time is e_* and the

corresponding area of an urban partition is s_*, the relative PV area $p(a)$ (Eq. (4)) and the relative PV capacity $p(e)$ (Eq. (5)) can be computed.

$$p(a) = \frac{a_c}{a_*} \mid e_i \geqslant e_{min} \tag{4}$$

$$p(e) = \frac{\int_0^t \int_0^a e_i}{e_*} \mid e_i \geqslant e_{min} \tag{5}$$

3.3. Optimizing the use of urban partitions

It is reasonable to build distributed PV generation on building surfaces to conserve valuable urban land, such as community roofs and skyscraper façades in commercial areas. In this study, the optimization is based on a community scale refined in a small urban area, which means that bare lands in suburbs will not be considered. Therefore, this study will exclusively utilize building surfaces for solar farming. Notably, the spatial distribution of solar irradiation on rooftops and façades can be significantly different even at the same instant of time because of different elevation angles and azimuths of the incoming solar irradiation, which are also affected by the surrounding urban morphology.

As rooftops can potentially provide continuously free space for deploying PV modules, utilizing rooftops is one of the most convenient ways in urban areas for solar harvesting. The advantage of using rooftops is also prominent during summer in that large elevation angles produce a high intensity of solar irradiation on rooftops and thus generate a large amount of electricity. However, solar capacity on rooftops may not be large enough if the generated electricity aims to completely offset the demand when there are multiple apartments in a resident building. In this consideration, this study proposes two alternatives, i.e., either seeking external-support (ES) by employing extra rooftops or building self-reliance (SR) by utilizing façades of the same building.

3.4. Optimization based on electricity demand

Since solar harvesting prefers an area where the accumulation of solar irradiation is both quantitatively large and spatially concentrated,
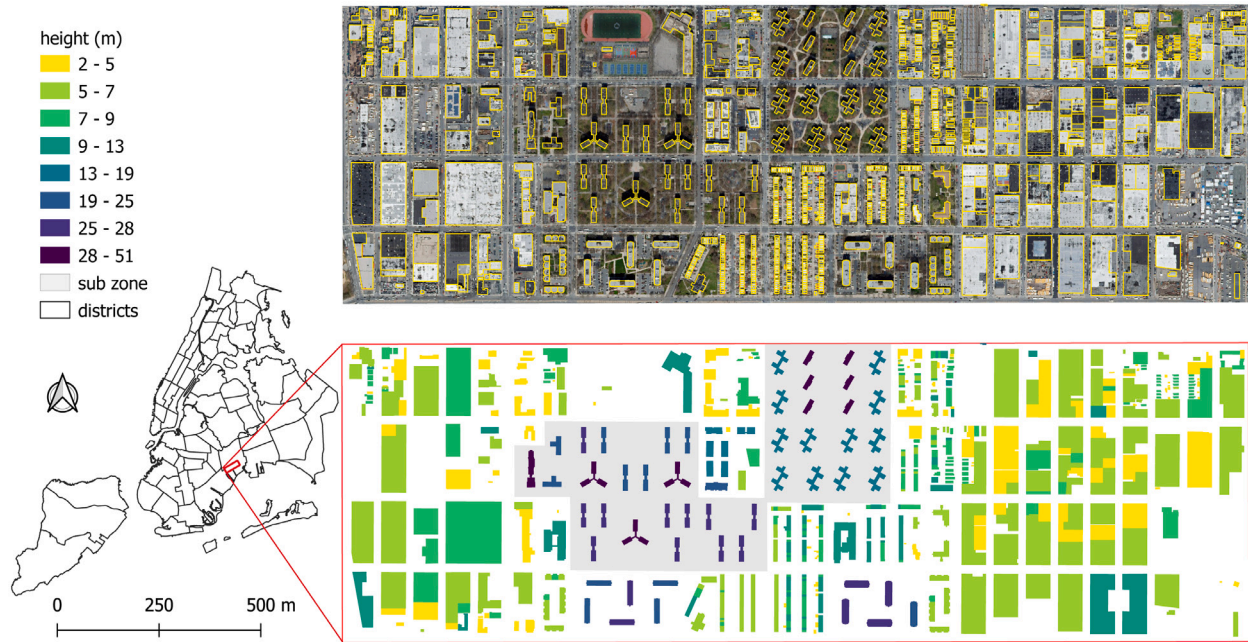
Fig. 2. The study area in the Brooklyn district of NYC. (For interpretation of the references to color in this figure legend, the reader is referred to the web version of this article.)

this study aims to maximize the accumulation of e_c (Eq. (6)) but minimize the sum of utilized area s_c (Eq. (7)). Therefore, solar PV capacity with large solar PV intensities is preferred to fulfill real electricity demand (Eq. (8)), which corresponds to the least amount of urban surfaces occupied by PV modules.

$$e_c = max(\int_0^t \int_0^s e_i) \mid e_i \geqslant e_{min} \tag{6}$$

$$a_c = min(\sum a) \mid e_i \geqslant e_{min} \tag{7}$$

$$e_c \geqslant e_{dmd} \tag{8}$$

3.5. Optimization based on economic feasibility assessment

Even though utilizing solar energy brings prominent benefits in environmental protection, it is essential to ensure that installing solar PV modules in a specific urban area is also economically feasible for the sustainable development of the photovoltaic industry. When transforming from solar irradiation to solar PV potential, this study assumes that the rated power of a brand new PV module is $0.2\ kW/m^2$ (i.e., corresponding to the transition efficiency $\varepsilon = 20\%$), which has been commonly attained in industry (Oberbeck et al., 2020). Also, this study anticipates a payback period of t years. This implies that if the payback period is too long, for example, more than 20 years, then the related urban area is abandoned for PV module deployment. According to NREL in the literature (Feldman et al., 2021), the installation cost is denoted by c_i ($/kW) and the O&M costs are denoted by c_m ($/kW/yr).

This study defines that the PV degradation rate is r_d and the increase rate of O&M costs is r_m every year, so that the transition efficiency and the O&M costs for t years since installation can be calculated in Eqs. (9) and (10), respectively. Then, the study forms a condition to ensure that a specific urban area is suitable for equipping with PV modules, by defining that the annual solar irradiation being harvested is u (kWh/m^2/yr) and the electricity rate is c ($/kWh). This study assumes that the generated electricity is transported to the national grid without a need of energy storage cost (Thanh et al., 2021; Tomar & Tiwari, 2017) and without any support from FiTs, implying that it will compete directly with the present electricity market. Eq. (11) presents that the profit obtained from a unit area (1 m^2) of the PV module is

equal to or more than the installation cost plus the O&M costs during t years, and t can be used as the expected payback year. Next, the total profit denoted by c_p can be calculated in Eq. (12), where $\sum u$ is the sum of *annual solar potential* and $\sum a$ is the total area equipped with the PV modules.

$$\varepsilon^* = \frac{\varepsilon - \varepsilon(1 - r_d)^t}{r_d} \tag{9}$$

$$c_m^* = \frac{c_m(1 + r_m)^t - c_m}{r_m} \tag{10}$$

$$c \cdot u \cdot \varepsilon^* \geqslant 0.2 \times c_i + 0.2 \times c_m^* \tag{11}$$

$$c_p = c \cdot \sum u \cdot \varepsilon^* - 0.2 \times c_i \cdot \sum a - 0.2 \times c_m^* \cdot \sum a \tag{12}$$

4. Empirical investigation

4.1. Study area

As one of the most densely urbanized areas with more than eight million population, New York City (NYC) consumed 49.201 TWh electricity in 2016 (NYC Open Data, 2016). The city government has aimed to supply at least 70% of electricity generated from renewable energy for the commitment of the Paris Agreement (City of New York, 2017). With this motivation, the city government has established an initiative to install 100 MW of solar PV modules on rooftops by 2025. As of 2018, the city has deployed 10.51 MW of solar capacity across 57 municipal buildings (NYC, 2018). To facilitate the solar deployment plan, the study thus explores the feasibility of pervasive solar energy generation in NYC.

Due to the difficulty of installing PV modules on skyscrapers in business districts such as Manhattan, this study focuses on a 2.23 km × 0.74 km urban area in Brooklyn (Fig. 2), which is a typical residential and commercial area with a reasonable density of buildings when compared to Manhattan. There are 1021 buildings totaling 507×10^3 m^2 in floor area. For easy computation and statistics, the study defined 3D point clouds at 1 m resolution, which means that a single point represents 1 m^2, resulting in 2.27 million 3D point clouds for the entire area.
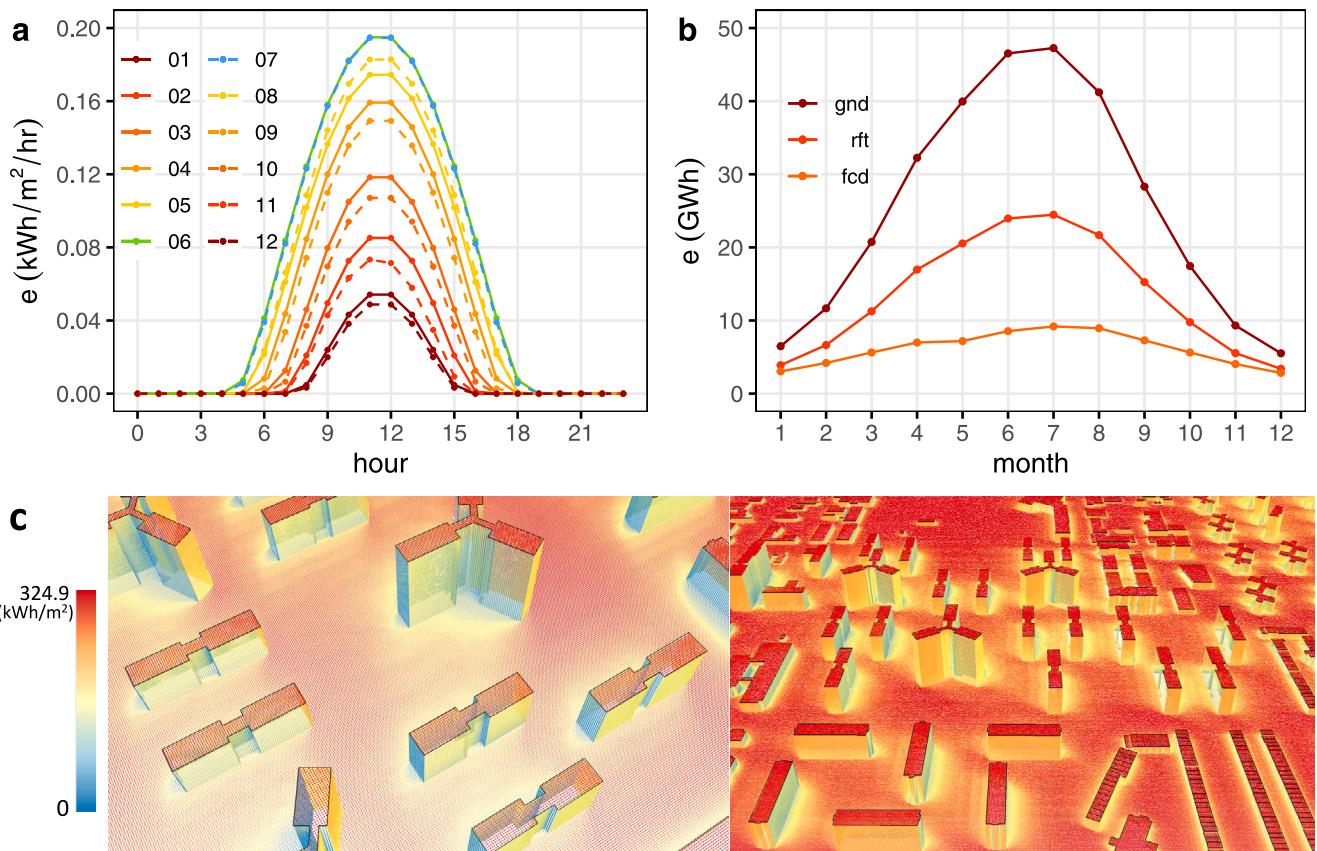
Fig. 3. Computation of solar PV potential. (a) Hourly solar PV intensity in different months of a year. (b) Accumulation of solar PV potential on three urban partitions in different months of a year. (c) Visualization of annual solar PV potential on 3D urban envelopes.

4.2. Data collection and computation

This study collected annual electricity usage data in 2019 (NYC Open Data, 2021a), which contains 122 buildings in the study area. Monthly electricity usage of buildings in 2019 was also collected, which is the latest data covering an entire calendar year (NYC Open Data, 2021b) and contains 40 residential buildings in the study area that have been marked with the gray background color in Fig. 2. Note that the two data sets only record electricity usage in part of the buildings so that buildings without records are not investigated in the study. In addition, footprints of buildings enriched with the height attribute were obtained from NYC Open Data (NYC Open Data, 2021c), which is conformed to the reality that rooftops in the study area are flat. Surrounding buildings outside the study area have a significantly low height with one or two floors only and the boundary of the study area includes streets with a width round 30 m. Therefore, it is unlikely that buildings outside the study area will affect the estimation of solar potential in this specific scenario, especially for the 40 residential buildings that are generally not along the boundary of the study areas.

The study used DBeaver 21.0 for the management of the database management system, PostgreSQL 13. Eclipse Java IDE was utilized to execute SQL queries in a series of databases for computing annual solar irradiation on urban envelopes. The computation was executed on a Windows 10 Enterprise, which has Intel(R) Core(TM) i7-6800K CPU @ 3.40 GMHz with 12 logical processors and 64 GB RAM.

5. Planning of solar PV capacity

5.1. Annual solar PV potential

First of all, the study computed the averaged hourly solar irradiation over a 12-month period (Fig. 3a) and accumulated solar irradiation of

Table 2
The electricity generation on three partitions and the total electricity demand in the whole study area and in the residential area during the entire year of 2019.

No.	Partition	e (GWh) whole area	e (GWh) residential area
1	Façades	73.518825	21.935322
2	Rooftops	163.357680	10.309823
3	Ground	306.707845	63.370407
4	Total	543.584350	95.615552
5	Demand	48.865723	22.888000

the same location over the year, which can be summarized on three urban partitions (i.e., rooftops, façades, and ground) (Fig. 3b). Then, annual solar irradiation on 3D point clouds is accumulated and visualized in Fig. 3c, which presents spatial heterogeneity of solar distribution on three partitions of urban envelopes, indicating the necessity of solar urban planning to harvest the greatest amount of solar PV potential with the least occupation of urban areas. It also reveals an important indicator that the largest annual PV intensity is 325 kWh/m^2. As a summary, solar PV potential on façades, rooftops, and the ground is 73, 163, and 306 GWh, resulting in a total potential of 543 GWh in 2019, which is fair enough if supporting the total demand of the 122 buildings at 48 GWh (Table 2). The 40 building surfaces with a total annual potential of 95 GWh are also able to support their demand at 22 GWh.

Considering that transforming land-use type, such as the change from parks to PV modules, could be challenging in many cities especially in a densely urbanized area, this study puts efforts on utilizing only building surfaces to examine the solar capacity. Fig. 4a presents building IDs on top of the building polygons, which also shows that the electricity consumption made by each building (in the gray area of Fig. 2) is approximately between 107.9×10^3 and 1848.7×10^3
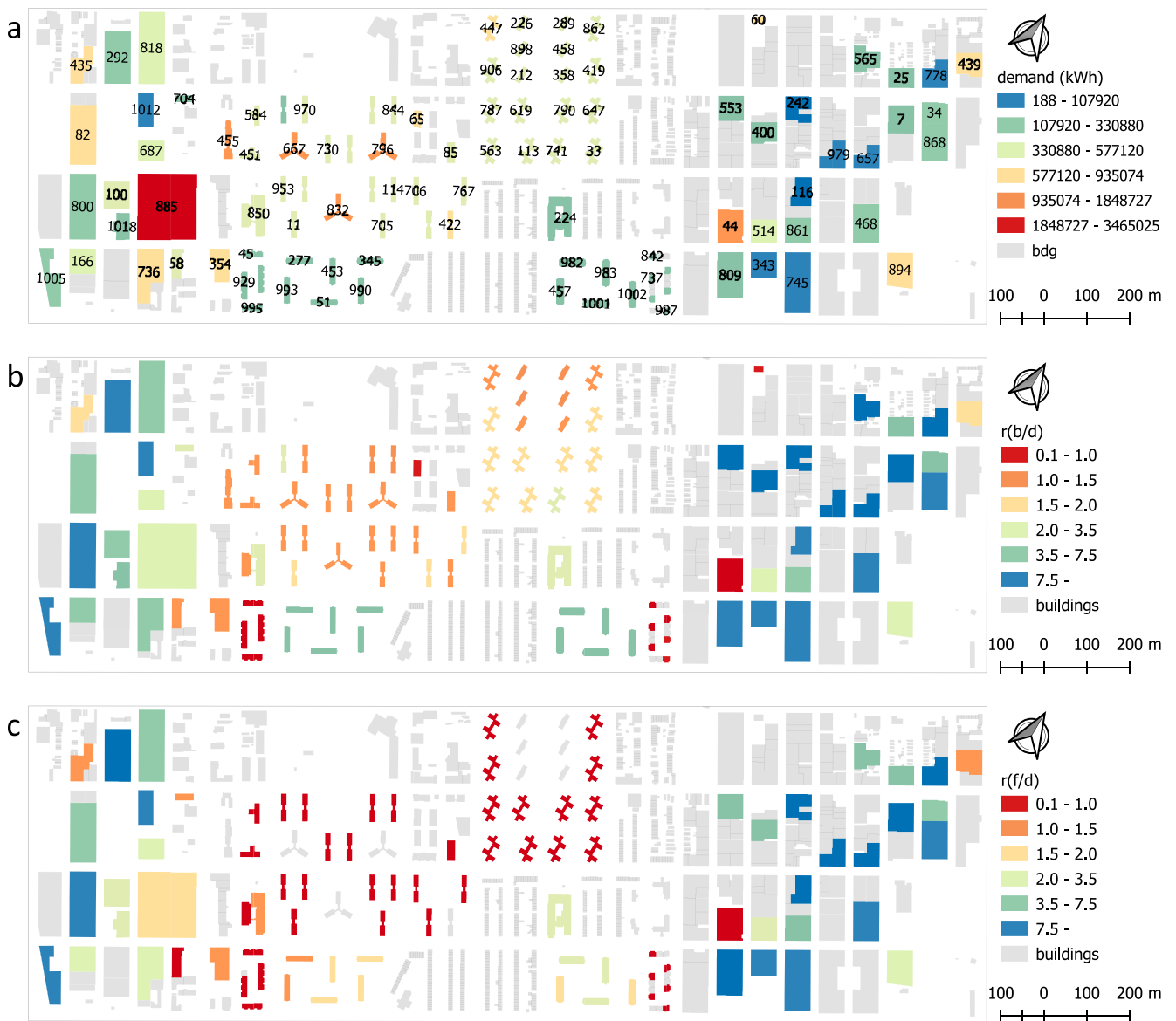
Fig. 4. The capability of solar PV potential to offset the electricity consumption. (a) Visualization of annual electricity consumption. (b) The rate between annual solar PV potential on the building surfaces and the consumption. (c) The rate between annual solar PV potential on the rooftops and the consumption.

kWh. The electricity consumption of residential buildings is medium compared with a few buildings having either little- or significant demand of electricity, which are supposed to be big shopping malls or warehouses. To investigate the capability of each building to support its own electricity demand, Fig. 4b presents the rate between annual solar PV potential on each building surface and the corresponding annual electricity consumption, denoted by $r(b/d)$. It demonstrates that the majority of buildings (81.15%) can achieve an SR architecture if all the solar potential on building surfaces can be utilized as their $r(b/d) \geqslant 1$, which includes all the 40 residential buildings having monthly demand records. However, in a strict scenario that harvesting solar PV potential only on rooftops (Fig. 4c), less than half of the buildings can achieve an SR architecture (45.08%), which also includes the 40 residential buildings.

Next, the study treats the 40 residential buildings as a building cluster that allows an independent solar PV system. To analyze the relation between supply and demand in each building, Fig. 5 plots monthly demand (dmd) and monthly solar PV potential on each rooftop (rft) and each building surface (bdg). Overall, solar PV potential on most building surfaces can theoretically offset the entire electricity

demand between March and October, while solar PV potential on almost all the rooftops can only offset part of the demand all year round. It is also noticed that four buildings ($bid = \{455, 667, 796, 832\}$) have monthly demands significantly larger than the other buildings, which are over 75×10^3 kWh probably because they are high-rise buildings with multiple apartments (Fig. 4a).

5.2. Relative distribution of solar PV capacity

People prefer collecting large solar PV intensities when they are concentrated in a single surface (e.g., a single rooftop) for ease of PV installation and O&M. In this consideration, the study summarizes spatial concentration of solar PV intensity on three urban partitions. Fig. 6a shows that, for 90% ($p(r) = 0.9$) of the rooftops, each rooftop has at least 80% ($p(a) = 0.8$) surface area with e_i equal or higher than 90% ($\delta = 0.9$) of the largest solar PV intensity. It also demonstrates that 85% ($p(g) = 0.85$) of the ground (Fig. 6b) and 10% ($p(f) = 0.1$) of the façades (Fig. 6c) have at least 20% surface area ($p(a) = 0.2$) satisfying $\delta = 0.9$. Furthermore, the other analysis is made to reveal the quantitative distribution of solar PV capacity. It is found that, for 80%
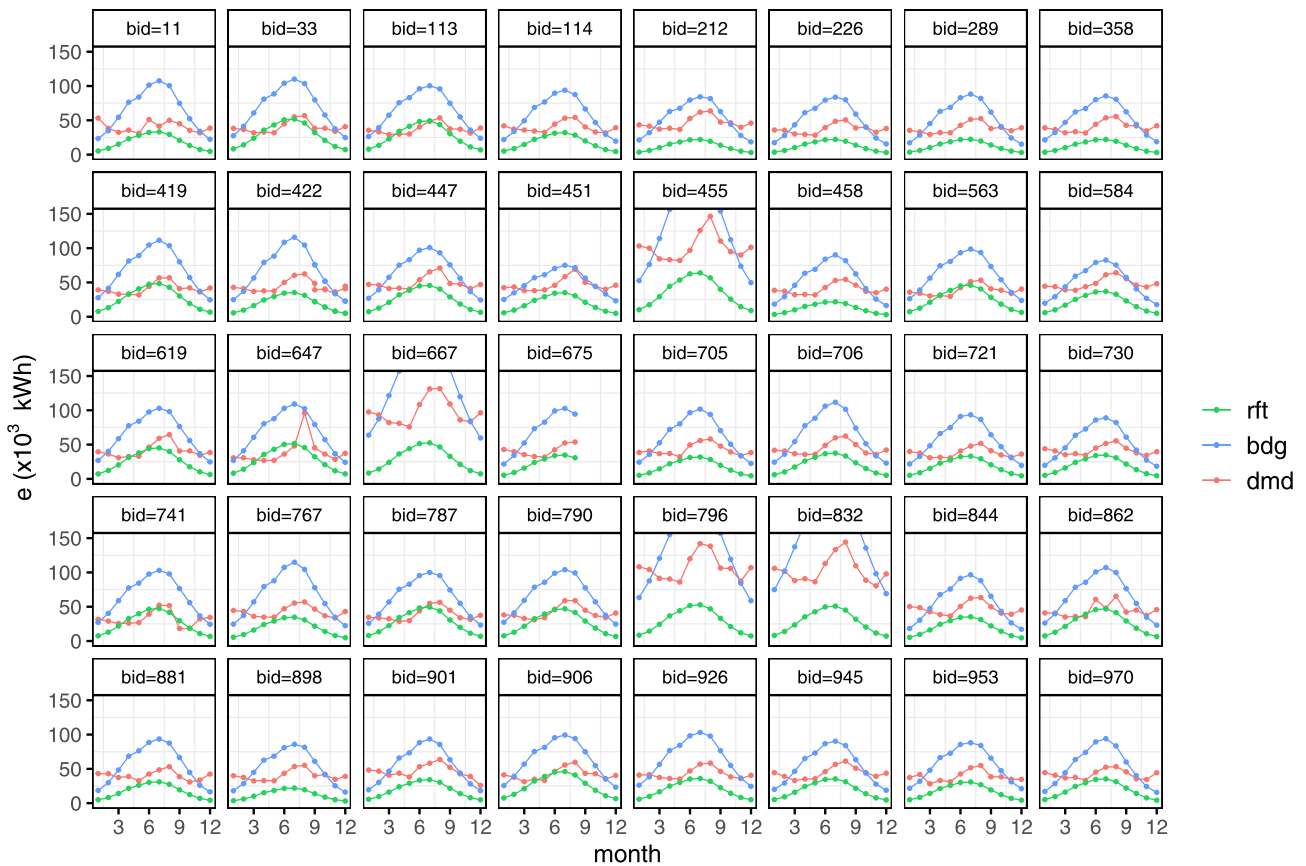
Fig. 5. Monthly electricity consumption (dmd) for the 40 buildings and the corresponding monthly solar PV potential on building surfaces (bdg) and rooftops (rft). Note that bid represents the building ID and the plot for $bid = 675$ is incomplete due to the missing information in the data source.

($p(r) = 0.8$) rooftops, almost 100% ($p(e) = 1$) of the solar PV potential on each rooftop can be harvested even if people plan to use the highest solar PV intensity with $\delta = 0.9$ (Fig. 7a). For 40% ground or façades, 62% of the solar PV potential on each ground surface (Fig. 7b) or 18% of the solar PV potential on each façade (Fig. 7c) can be utilized when $\delta = 0.9$. According to the accumulation of solar PV potential throughout the year, the largest annual solar PV intensity on rooftops, ground, and façades is 324.9, 324.9, and 260.3 kWh/m^2, respectively. Since rooftops have the largest $p(a)$ and $p(e)$ compared with the ground and façades under the same condition, the analysis implies that rooftops have the most concentrated solar PV intensity followed by ground and façades.

5.3. Absolute distribution of solar PV capacity

As discussed in Section 3.2, there is a trade-off between utilizing the largest solar PV intensity and harvesting the largest solar PV capacity. Thus, this study investigates the effect of utilizing different solar PV intensities on solar PV harvesting, considering that the distribution of solar potential is heterogeneous on urban envelopes. It is discovered that e_i increases from 32.5 to 292.4 kWh/m^2 when δ grows from 0.1 to 0.9 with a constant interval of 0.1 (Fig. 8a); accordingly, the total solar PV capacity e_c decreases from 31.84 to 10.30 GWh on surfaces of the 40 buildings. Notably, the total annual electricity consumption is $e_d = 22.89$ GWh, which means that the 40 buildings can theoretically attain self-sufficiency for electricity demand with $\delta \leqslant 0.4$.

Alternatively, rooftops may be utilized only to harvest solar PV potential. It is found that the solar PV capacity is with $e_c = 10.31$ GWh if only utilizing rooftops of the 40 buildings (i.e., $n = 0$ in the x-axis of Fig. 8b), which is far away from getting balanced with the real demand. Thus, employing additional rooftops might be an efficient solution to meet actual electricity demand. With an descending order of solar PV potential on the other rooftops, the total PV potential is accumulated on eight additional rooftops (i.e., $n = \{1, \ldots, 8\}$ in the x-axis of Fig. 8b). It is demonstrated that the three extra rooftops may help offset the entire electricity consumption, which is supposed to be large in area since they can generate a large amount of electricity at $(e_d - e_c)|_{n=0} = 12.38$ GWh.

It is also vital for executable solar urban planning to accurately identify the total surface area to be equipped with PV modules to harvest solar PV potential. In the SR scenario, the total available area of building surfaces decreases from nearly 200×10^3 to 31.86×10^3 m^2 with the increase of δ (Fig. 9a). As building surfaces can be partitioned by façades and rooftops, the total areas in the two partitions are also presented. It shows that usable areas on façades decrease but the areas on rooftops remain the same with the increase of δ. This suggests a spatially heterogeneous distribution of solar PV potential on façades that have both solar abundant areas and long-term shadow areas. In contrast, the distribution of solar PV potential on rooftops is homogeneous and consistent with the largest solar PV intensity; this is because most rooftops in the study area are flat and shadow generated by surrounding buildings does not project onto rooftops most of the time, benefiting from low building densities. In the ES scenario, available areas on rooftops increase steadily from 31.90×10^3 to 115.80×10^3 m^2 with the increase of the number of external buildings n (Fig. 9b). Based on the above analysis, the planned PV capacity can generate 23.81 GWh when $\delta = 0.4$ and 32.26 GWh when $n = 6$ to achieve a complete offset of electricity consumption between March and October (Fig. 8), and the corresponding total area needed is 111.76×10^3 m^2 and 99.50×10^3 m^2 (Fig. 9). The above results suggest that the ES architecture is superior because it can generate more electricity with a smaller area of PV modules.
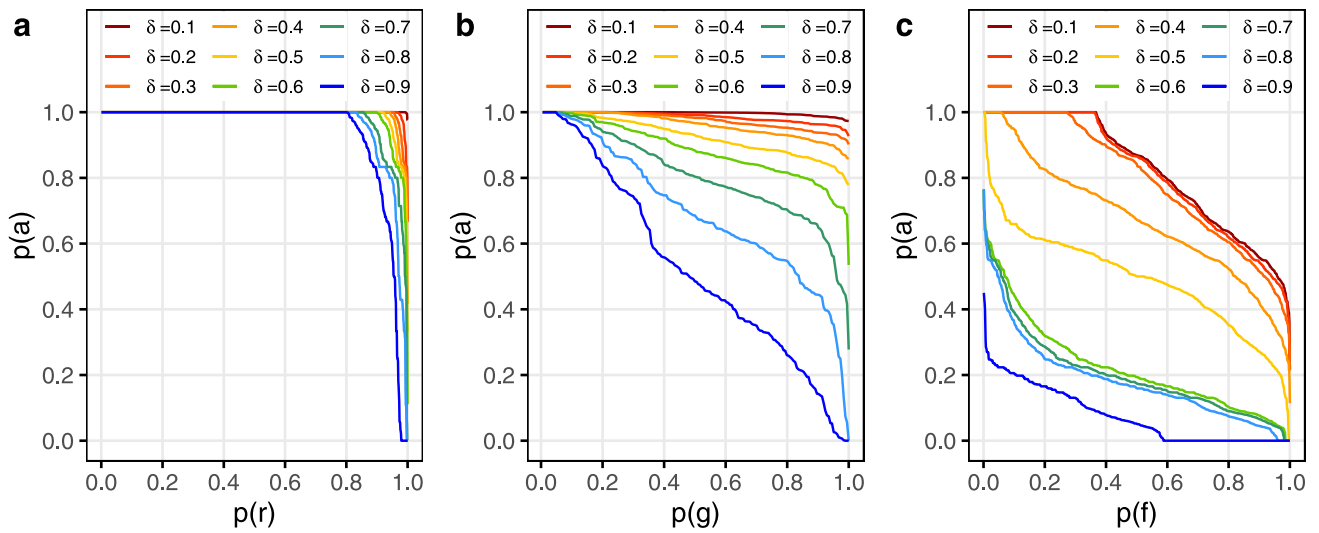
Fig. 6. Relative distribution of the PV area. $p(a)$ is the proportion of the total PV area (Eq. (4)) when the PV capacity $e_c \geqslant \delta \cdot max(e_i)$, where $\delta = \{0.1, 0.2, \ldots, 0.9\}$. (a) Rate of rooftops $p(r)$. (b) Rate of ground $p(g)$. (c) Rate of façades $p(f)$.
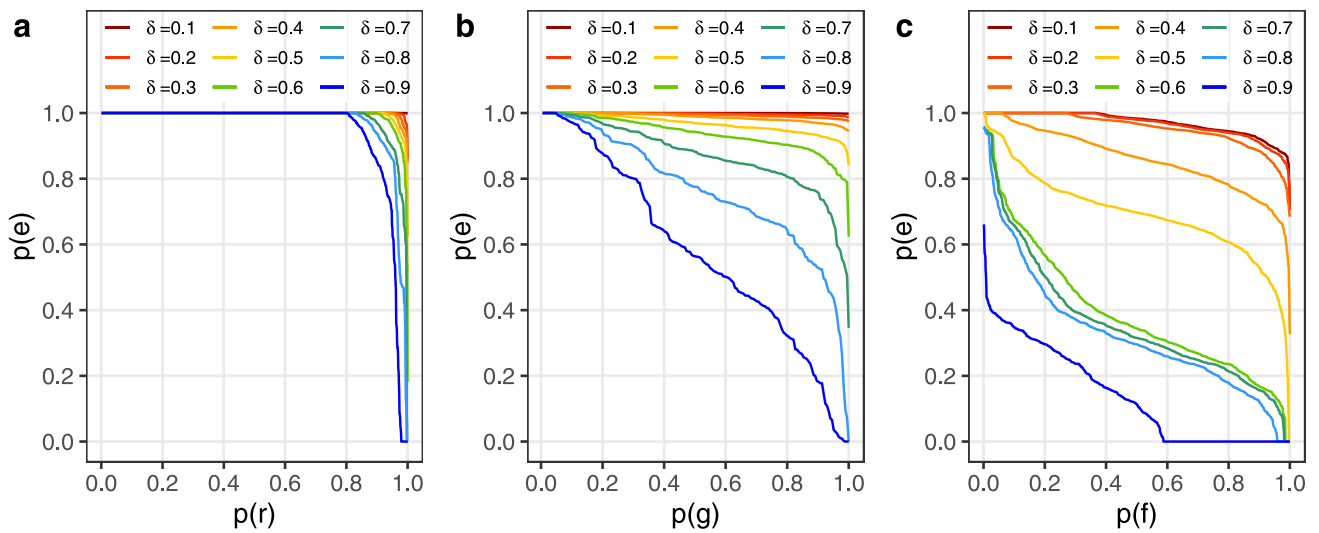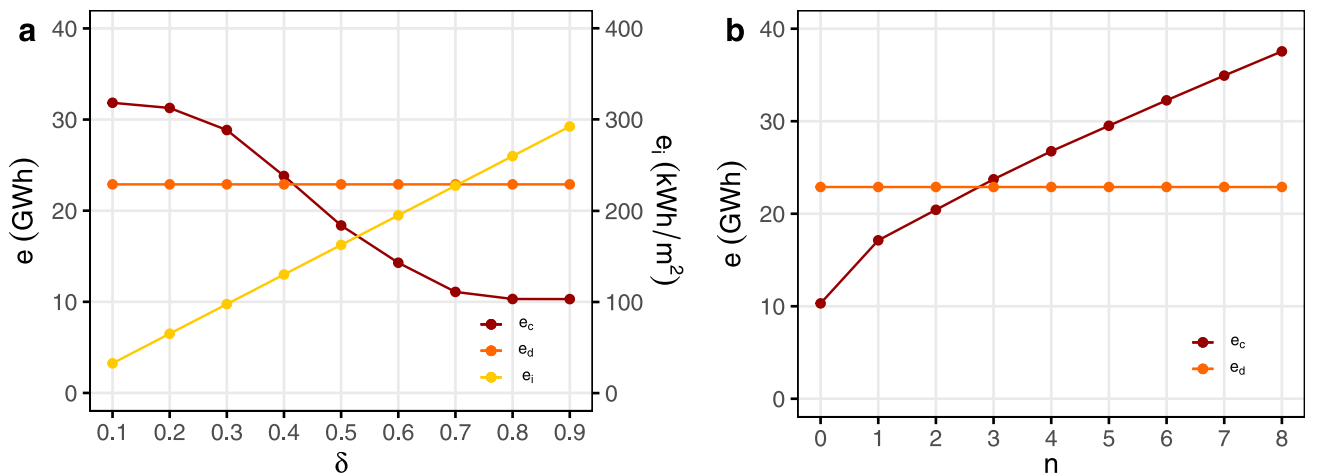

Fig. 7. Relative distribution of the PV capacity. $p(e)$ is the proportion of the total PV capacity (Eq. (5)) when the PV capacity $e_c \geqslant \delta \cdot max(e_i)$, where $\delta = \{0.1, 0.2, \ldots, 0.9\}$. (a) Rate of rooftops $p(r)$. (b) Rate of ground $p(g)$. (c) Rate of façades $p(f)$.

Fig. 8. Availability of solar PV potential. (a) The total solar PV potential when utilizing a series of solar PV intensities. (b) The total solar PV potential when utilizing a number of additional rooftops.
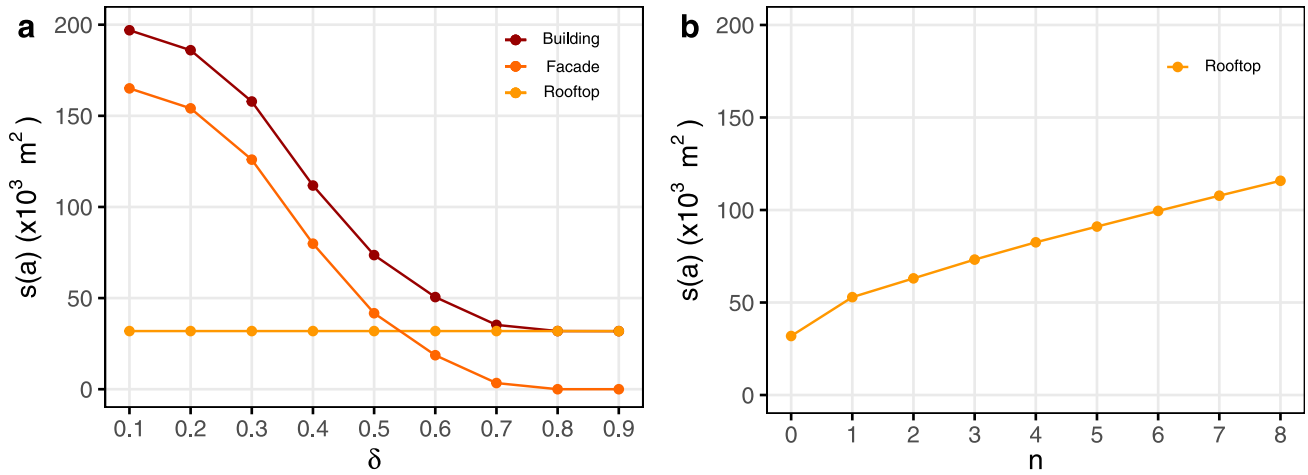
Fig. 9. Available areas for the installation of PV modules. (a) Available areas in the SR scenario. (b) Available areas in the ES scenario.
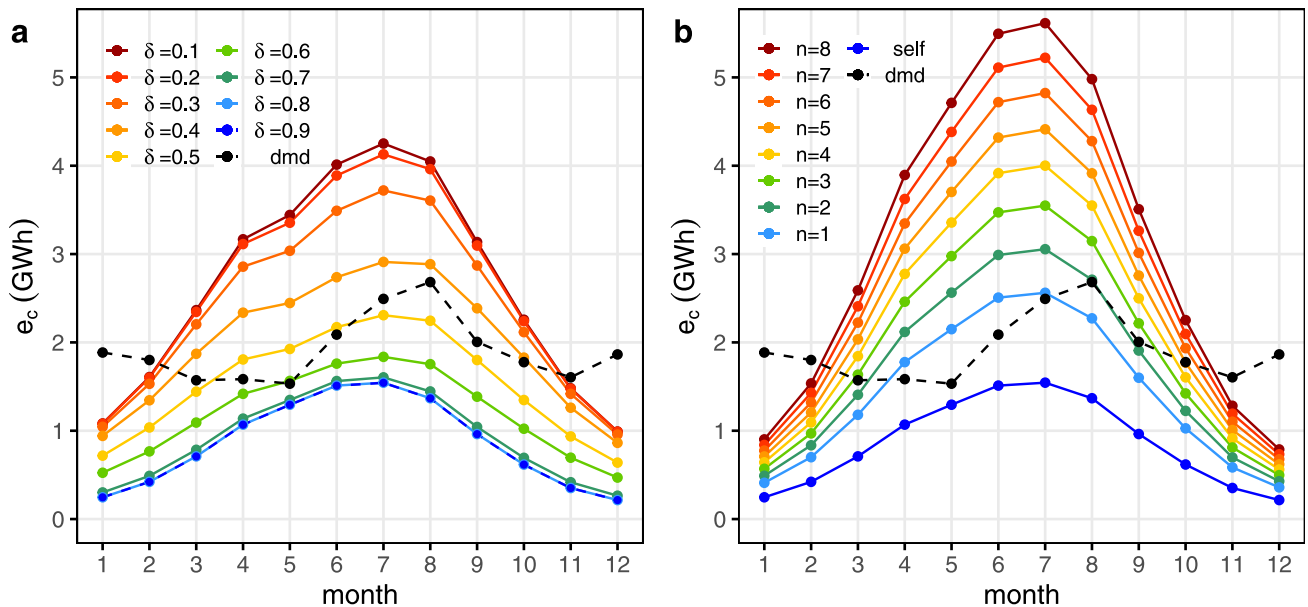

Fig. 10. Variation of solar PV potential to be harvested in different months of a year. (a) Variation when equipping PV modules on their own building surfaces. (b) Variation when equipping PV modules on rooftops of surrounding buildings. (For interpretation of the references to color in this figure legend, the reader is referred to the web version of this article.)

5.4. Optimization based on monthly solar PV potential

As this study aims to achieve a self-sufficient micro-grid in the community by generating green electricity from PV modules, it is imperative to investigate the availability of solar PV potential a different time of year after an overview of the solar PV capacity. According to the dashed black curve (Fig. 10a), it is noticed that two consumption peaks at 1.88 GWh in January and 2.68 GWh in August for the 40 residential buildings. This might be because of the cooling and heating purposes in summer and winter. In the SR scenario when equipping PV modules on their own building surfaces including façades and rooftops, it is found that this strategy can offset the entire electricity consumption between March and October as the generated electricity represented by curves with $\delta \leqslant 0.4$ and $e_{max} = 424.9$ kWh/yr is always larger than the consumption (Fig. 10a). However, it is difficult to achieve the self-sufficient objective between November and the following February since it can only offset part of the consumption even utilizing the largest

solar PV capacity with $\delta = 0.1$. This is mainly because of the seasonal fluctuation that solar intensity is low and daytime is short during late winter and early spring for NYC located at a latitude of $40.71°$.

In the ES scenario when equipping PV modules on their own and other rooftops, it presents that their own rooftops cannot offset the entire electricity consumption all year round as the solid blue curve referenced as the baseline is always below the dashed black curve (Fig. 10b). With a descending order of the solar capacity on rooftops, this study explores the total solar PV capacity by using an accumulative number of surrounding rooftops denoted by $n = \{1, \ldots, 8\}$ (Fig. 10b), which are the same rooftops essentially as discussed in Fig. 8b. Note that all the area on these rooftops has at least 80% ($\delta = 0.8$) of the largest solar PV intensity ($e_{max} = 324.9$ kWh/m^2/yr). It demonstrates that six additional rooftops are needed for the installation of PV modules to fully support the electricity demand between March and October, while it only needs three additional rooftops if just achieving an SR between March and September. Notably, abundant electricity has

Table 3
Solar PV degradation and the increase rate of O&M costs for a life cycle of 25 years.

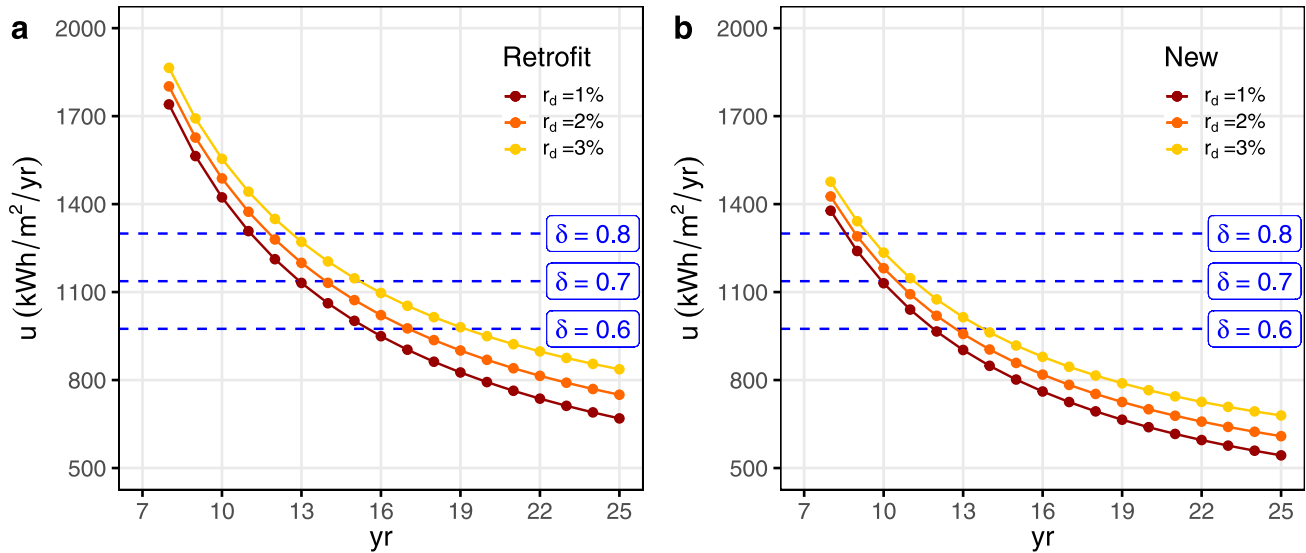| No.	r_d	Decrease over 25 years	Output after 25 years	r_m	Increase over 25 years	Cost after 25 years
1	1%	21.43%	78.57%	0.30%	7.45%	107.45%
2	2%	38.42%	61.58%	0.30%	7.45%	107.45%
3	3%	51.86%	48.14%	0.30%	7.45%	107.45%

Fig. 11. The payback period for deploying PV modules subject to solar PV intensity to be harvested. (a) Retrofits on existing buildings. (b) New construction on being built buildings.

already remained with the support of three additional rooftops even after deducting the largest electricity consumption in August.

5.5. Optimization based on techno-economic assessment

It is reasonable to assume annual PV degradation rate $r_d = 1\%$ according to previous studies (Chandel et al., 2015; Forniés et al., 2021; Ishii & Masuda, 2017). The study also sets $r_d = 2\%$ and $r_d = 3\%$ for comparative analysis and assumes that the O&M costs increase by 0.3% very year (Table 3). The averaged residential electricity rate c is 0.2321 $/kWh in NYC (Electricity Local, 2021), and this study maintains this price constant across a 25-year life cycle. The installation cost c_i is 2970 $/kW for retrofits on existing buildings and 2320 $/kW for deploying on being constructed new buildings, and the O&M costs c_m are 18.55 $/kW/yr according to the latest statistics made by NREL (Feldman et al., 2021).

Based on Eq. (11), the study investigates the minimum *annual solar potential* (u) to be harvested to return the investment in an appropriate period without the support from FiT. For each individual PV module having 1 m^2 and for $r_d = 1\%$, the retrofit scenario shows that the *longest* payback period is approximately 11 years when $\delta = 0.8$, 13 years when $\delta = 0.7$, and 16 years when $\delta = 0.6$ (Fig. 11a). Note that these should be the longest payback period because δ corresponds to the minimum threshold to harvest solar irradiation when installing PV modules. In comparison, it takes three years longer to recoup the investment when utilizing solar irradiation with $\delta = 0.6$ but $r_d = 3\%$. In the other scenario when constructing PV modules on new buildings, the payback period is 4 years shorter, i.e., 12 years, than retrofits when $\delta = 0.6$ and $r_d = 1\%$, owing to lower O&M costs (Fig. 11b).

Furthermore, this study considers that retrofit is the actual situation of our study because rooftops will be retrofitted and PV modules will be installed on existing buildings. Thus, a large amount of electricity can be generated to achieve an acceptable payback period when setting $\delta = 0.6$ according to Fig. 11a, which requires *annual solar irradiation* to be collected is *at least* 974.4 kWh/m^2/yr. In this case, a solar PV system

with the SR architecture can generate an amount of 14.29 GWh/yr electricity in the first year, leading to an offset of 62.42% of the total demand in 2019. In comparison, by developing the ES architecture, a total amount of electricity at 37.55 GWh/yr can be generated in the first year that corresponds to 164.07% of the total demand in 2019, which can entirely offset the demand between March and October. In the other aspect, an area of 50,546 m^2 will be used for deploying PV modules on building surfaces (SR), decomposed by 18,648 m^2 on façades (7.86% of the building surfaces) and 31,898 m^2 on rooftops (13.45% of the building surfaces); in contrast, it requires an area of 115,798 m^2 for the equipment of PV modules when only utilizing rooftops (ES).

The above analysis provides a guideline to compute the net profit of the planned PV system during the whole life cycle based on Eq. (12). This study further investigates the changes of net profit over time when $\delta = 0.6$. As a result, SR and ES will be able to make a profit since the 12th year (Fig. 12a) and the 10th year (Fig. 12a) in all situations, respectively, and both can obtain a considerable amount of profit when the planned PV system works till the last year. In detail, the payback period for SR is slightly longer than ES because SR also utilizes façades for solar farming, resulting in the harvested solar irradiation being relatively lower. Also, the total net profit for SR is less than half of the ES because its construction size is also notably smaller. Even though the initial investment is large (i.e., nearly 30 million for SR and 60 million for ES) and the return period is significantly long, both architectures explicitly show a promisingly total profit at 38.8 million USD for SR and 113.7 million USD for ES when $r_d = 1\%$. Even in the worst case that $r_d = 3\%$, SR and ES can earn 24.0 million and 74.9 million USD, respectively.

Finally, the study visualizes spatial locations of the PV modules to be installed for solar farming when $\delta = 0.6$. It presents that the SR architecture determines PV modules on all the 40 residential rooftops and part of the solar-facing façades that are located at high altitudes little shadow blocking (Fig. 13a,b). In contrast, ES also determines PV modules on all the 40 residential rooftops and with external support
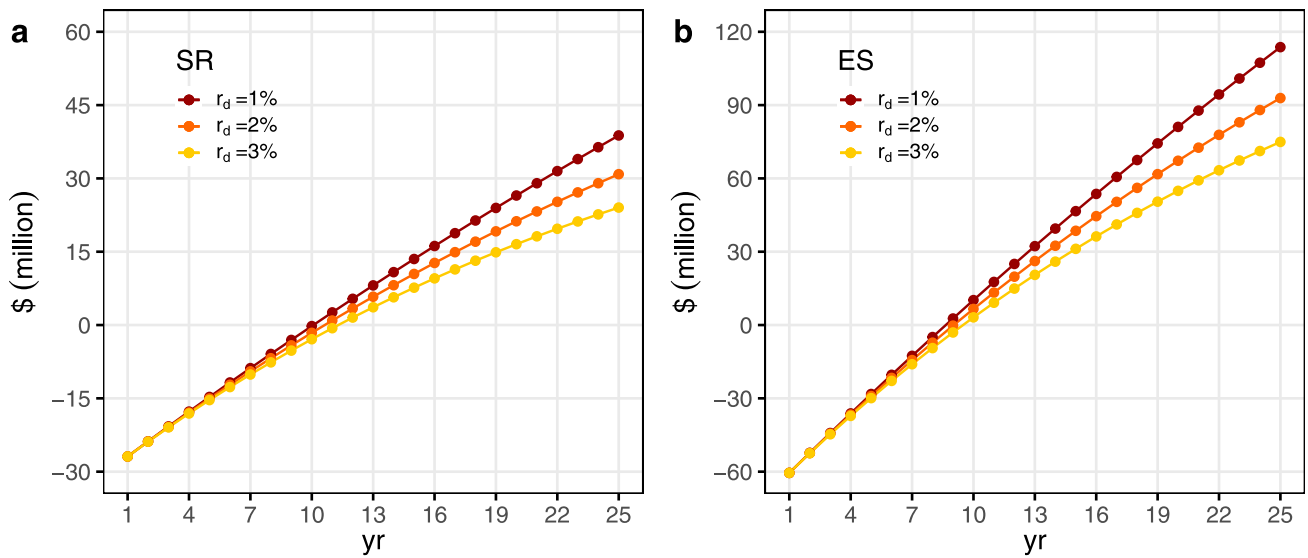
Fig. 12. The net profit for deploying PV modules with $\delta = 0.6$ during the whole life cycle of 25 years. (a) Retrofits with the SR architecture. (b) Retrofits with the ES architecture.
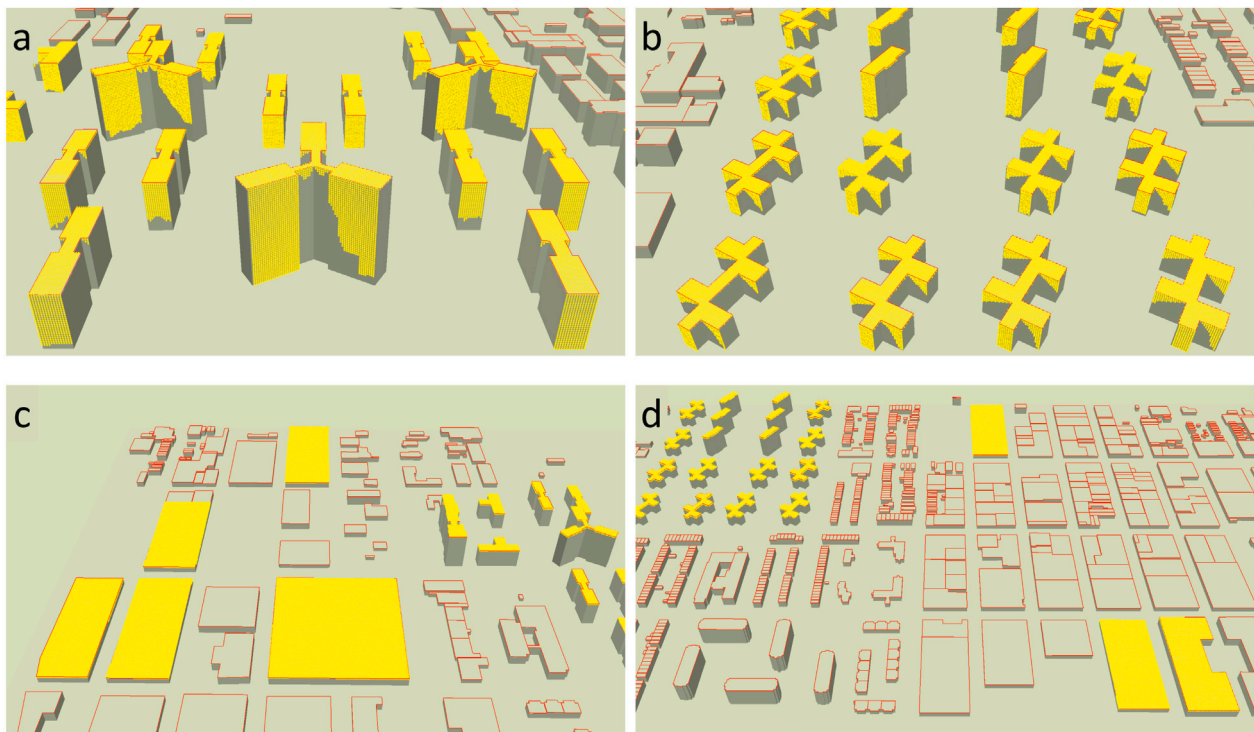

Fig. 13. Spatial location of planned PV modules presented by 3D point clouds in yellow. (a,b) PV location for SR. (c,d) PV location for ES. (For interpretation of the references to color in this figure legend, the reader is referred to the web version of this article.)

from eight large rooftops (Fig. 13c,d), which indicates an easier operation and management because these solar PV plants have fewer discrete distributions.

6. Discussion and conclusion

Because of seasonal variation of solar irradiation, the generated electricity is abundant between March and October but inadequate between November and the next February to entirely offset real electricity demand. The study does not estimate the electricity storage cost based on the assumption that the generated electricity is transported to the national grid immediately. This assumption also brings a possibility of creating a dynamic balance between demand and supply that the PV

system borrows electricity during winter and returns the same amount during summer. On this basis, the proposed PV installing plan can significantly or even fully satisfy the real electricity demand of local residences. This study assumes that PV vendors would construct and operate the PV system, resulting in O&M costs, which will not be affected by the governance because the PV installation does not occupy urban property and the economic assessment does not require subsidy from FiT. If the operation and maintenance are made by the occupants of the buildings, it will be even more profitable as O&M costs are eliminated.

Based on the current study area, the results suggest that ES outperforms SR because ES can generate a larger amount of electricity but a smaller occupation of building surfaces. However, it does not mean

that ES is always advantageous in all situations. For instance, because Manhattan is fulfilled with a high density of skyscrapers, façades at a high altitude should maintain a majority of solar PV potential as façade areas are significantly larger than rooftop areas. Thus, SR can still be an appropriate solution by deploying semi-transparent PV modules on façades in a different urban area. This highlights the necessity of comparing both architectures for solar PV planning.

NYC has no advantages in using solar energy in three aspects since it has relatively high latitude, high densities of building clusters, and high cost of PV installation and O&M. On this premise, this study estimated economic feasibility by taking three rigorous constraints into account: PV efficiency degradation, an rise in operation and O&M expenses, and a constant electricity rate without FiT support throughout the life cycle. It is worth noting that the O&M costs have been greater than 300 $/kW/yr from the 16th year of the implementation when $r_m = 0.30\%$. Nonetheless, the results demonstrate that the study area is favorable to utilize solar energy in consideration of electricity generation and economic feasibility. This is inspiring to encourage researchers, urban planners, environmentalists, and investors to promote the development of the distributed PV system in other cities with similar socioeconomic conditions and even better geographical conditions, such as Hong Kong and Singapore located at a lower latitude. In addition, the proposed spatio-temporal analytic model for the optimization of PV provision can be used in different cities as the model is adaptive to new data sets without the need for modification, indicating a profound impact in developing sustainable cities.

In this study, rooftops are modeled by 3D horizontal polygons, which conforms to the fact that the selected study area is packed with flat rooftops. This is contrast to conventional American residential neighborhoods, which are mostly made up of individual houses with tiled roofs. Nevertheless, our solar estimation model has been able to compute solar irradiation on tiled rooftops when a fine scale of the 3D building model with an inclination angle is provided. In the other aspect, developing PV systems on being built buildings is superior to retrofitting on existing buildings, mainly benefiting from saving of installation cost. Therefore, it is persuasive to promote PV modules when constructing new buildings.

The study contains three uncertainties. First, because 3D building model lacks precise structures, this study may overestimate solar PV capacity on façades because structures such as windows and balconies are not differentiated in our estimation for installing PV modules. Second, this study estimates solar PV capacity based on horizontal surfaces. This means that the optimum inclination angle of PV modules has not been considered when estimating solar PV capacity, which requires additional spatio-temporal modeling by considering shadow effects between PV arrays with optimized gaps. Nevertheless, results obtained from this study are reliable, supposing that the inclination angle is zero. Third, real electricity demand used in this study is only based on one-year historical data, which may not be statistically significant. Consequently, the planned electricity supply may deviate from the future demand, owing to various months and different buildings. To address the uncertainties, future work can use deep learning-based semantic segmentation to extract windows and balconies from street-view images for customized PV planning, optimize PV layouts by modeling the shading effect between PV arrays, and predict future electricity demand using the Seasonal Autoregressive Integrated Moving Average with eXogenous factors (SARIMAX), which incorporates seasonal and periodical variations, linear trends, and residuals into the prediction (Wong et al., 2021).

In conclusion, the proposed spatio-temporal analytic method is effective to optimize PV provision by incorporating real electricity demand from customers, heterogeneous supply of solar potential on urban envelopes, and economic feasibility with the decrease of PV efficiency, an increase of O&M costs, and constant of electricity price. The estimated solar potential is reliable as the study models atmospheric effects from the historical cloud over and geometrical effects from

urban morphology that significantly determines the spatial distribution of solar irradiation. The study suggests that building clusters in NYC with a reasonable density are suitable to be used for solar farming. This study is encouraging to promote distributed solar farming in other global cities since the estimated profit is inspirational and the proposed optimization method is universal for diverse cities.

Declaration of competing interest

The authors declare that they have no known competing financial interests or personal relationships that could have appeared to influence the work reported in this paper.

Acknowledgments

References

ArcGIS Pro (2021). *Points solar radiation (Spatial analyst)*. Accessed 30 June 2021 https://pro.arcgis.com/en/pro-app/latest/tool-reference/spatial-analyst/points-solar-radiation.htm.

Baum, Z., Palatnik, R. R., Ayalon, O., Elmakis, D., & Frant, S. (2019). Harnessing households to mitigate renewables intermittency in the smart grid. *Renewable Energy, 132*, 1216–1229.

Bianchi, M., Branchini, L., Ferrari, C., & Melino, F. (2014). Optimal sizing of grid-independent hybrid photovoltaic–battery power systems for household sector. *Applied Energy, 136*, 805–816.

Calcabrini, A., Ziar, H., Isabella, O., & Zeman, M. (2019). A simplified skyline-based method for estimating the annual solar energy potential in urban environments. *Nature Energy, 4*(3), 206–215.

Catita, C., Redweik, P., Pereira, J., & Brito, M. C. (2014). Extending solar potential analysis in buildings to vertical facades. *Computers & Geosciences, 66*, 1–12.

Chandel, S. S., Nagaraju Naik, M., Sharma, V., & Chandel, R. (2015). Degradation analysis of 28 year field exposed mono-c-Si photovoltaic modules of a direct coupled solar water pumping system in western Himalayan region of India. *Renewable Energy, 78*, 193–202.

Chu, S., & Majumdar, A. (2012). Opportunities and challenges for a sustainable energy future. *Nature, 488*(7411), 294–303.

City of New York (2017). *Aligning New York City with the Paris agreement*. Accessed 30 June 2021 https://www1.nyc.gov/assets/sustainability/downloads/pdf/publications/1point5-AligningNYCwithParisAgrmt-02282018_web.pdf.

Creutzig, F., Baiocchi, G., Bierkandt, R., Pichler, P. P., & Seto, K. C. (2015). Global typology of urban energy use and potentials for an urbanization mitigation wedge. *Proceedings of the National Academy of Sciences of the United States of America, 112*(20), 6283–6288.

Cristea, C., Cristea, M., Birou, I., & Tîrnovan, R. A. (2020). Economic assessment of grid-connected residential solar photovoltaic systems introduced under Romania's new regulation. *Renewable Energy, 162*, 13–29.

Dasari, H. P., Desamsetti, S., Langodan, S., Attada, R., Kunchala, R. K., Viswanadha-palli, Y., Knio, O., & Hoteit, I. (2019). High-resolution assessment of solar energy resources over the Arabian Peninsula. *Applied Energy, 248*, 354–371.

Dike, V. N., Chineke, T. C., Nwofor, O. K., & Okoro, U. K. (2012). Optimal angles for harvesting solar electricity in some African cities. *Renewable Energy, 39*(1), 433–439.

Dyson, M. E. H., Borgeson, S. D., Tabone, M. D., & Callaway, D. S. (2014). Using smart meter data to estimate demand response potential, with application to solar energy integration. *Energy Policy, 73*, 607–619.

Electricity Local (2021). Accessed 30 June 2021 https://www.electricitylocal.com/states/new-york/new-york/.

Erdélyi, R., Wang, Y., Guo, W., Hanna, E., & Colantuono, G. (2014). Three-dimensional SOlar RAdiation Model (SORAM) and its application to 3-D urban planning. *Solar Energy, 101*, 63–73.

Feldman, D., Ramasamy, V., Fu, R., Ramdas, A., Desai, J., & Margolis, R. (2021). *U.S. solar photovoltaic system cost benchmark: Q1 2020*. https://www.nrel.gov/docs/fy21osti/77324.pdf.

Forniés, E., del Cañizo, C., Méndez, L., Souto, A., Pérez Vázquez, A., & Garrain, D. (2021). UMG silicon for solar PV: From defects detection to PV module degradation. *Solar Energy, 220*, 354–362.

Hofierka, J., & Zlocha, M. (2012). A new 3-D solar radiation model for 3-D city models. *Transactions in GIS, 16*(5), 681–690.

Huang, S., Rich, P. M., Crabtree, R. L., Potter, C. S., & Fu, P. (2008). Modeling monthly near-surface air temperature from solar radiation and lapse rate: Application over complex terrain in yellowstone national park. *Physical Geography, 29*(2), 158–178.

Ishii, T., & Masuda, A. (2017). Annual degradation rates of recent crystalline silicon photovoltaic modules. *Progress in Photovoltaics: Research and Applications, 25*(12), 953–967.

Jakubiec, J. A., & Reinhart, C. F. (2013). A method for predicting city-wide electricity gains from photovoltaic panels based on LiDAR and GIS data combined with hourly Daysim simulations. *Solar Energy, 93*, 127–143.

Kalder, J., Annuk, A., Allik, A., & Kokin, E. (2018). Increasing solar energy usage for dwelling heating, using solar collectors and medium sized vacuum insulated storage tank. *Energies, 11*(7), 1832.

Kan, Z., Wong, M. S., & Zhu, R. (2020). Understanding space–time patterns of vehicular emission flows in urban areas using geospatial technique. *Computers, Environment and Urban Systems, 79*, Article 101399.

Kettani, M., & Bandelier, P. (2020). Techno-economic assessment of solar energy coupling with large-scale desalination plant: The case of Morocco. *Desalination, 494*, Article 114627.

Li, Y., Ding, D., Liu, C., & Wang, C. (2016). A pixel-based approach to estimation of solar energy potential on building roofs. *Energy and Buildings, 129*, 563–573.

Li, W. T., Tushar, W., Yuen, C., Ng, B. K. K., Tai, S., & Chew, K. T. (2020). Energy efficiency improvement of solar water heating systems – An IoT based commissioning methodology. *Energy & Buildings, 224*, Article 110231.

Li, T. X., Wang, R. Z., & Yan, T. (2015). Solid-gas thermochemical sorption thermal battery for solar cooling and heating energy storage and heat transformer. *Energy, 84*, 745–758.

Liang, J., Gong, J., Li, W., & Ibrahim, A. N. (2014). A visualization-oriented 3D method for efficient computation of urban solar radiation based on 3D–2D surface mapping. *International Journal of Geographical Information Science, 28*(4), 780–798.

Liang, J., Gong, J., Zhou, J., Ibrahim, A. N., & Li, M. (2015). An open-source 3D solar radiation model integrated with a 3D Geographic Information System. *Environmental Modelling & Software, 64*, 94–101.

Lim, K. Z., Lim, K. H., Wee, X. B., Li, Y., & Wang, X. (2020). Optimal allocation of energy storage and solar photovoltaic systems with residential demand scheduling. *Applied Energy, 269*, Article 115116.

Lin, B., & Li, Z. (2020). Spatial analysis of mainland cities' carbon emissions of and around Guangdong-Hong Kong-Macao Greater Bay area. *Sustainable Cities and Society, 61*, Article 102299.

Lindberg, F., Jonsson, P., Honjo, T., & Wästberg, D. (2015). Solar energy on building envelopes – 3D modelling in a 2D environment. *Solar Energy, 115*, 369–378.

Lobaccaro, G., Carlucci, S., Croce, S., Paparella, R., & Finocchiaro, L. (2017). Boosting solar accessibility and potential of urban districts in the Nordic climate: A case study in Trondheim. *Solar Energy, 149*, 347–369.

Ma, S., Goldstein, M., Pitman, A. J., Haghdadi, N., & MacGill, I. (2017). Pricing the urban cooling benefits of solar panel deployment in Sydney, Australia. *Scientific Reports, 7*(1), 43938.

Mangiante, M. J., Whung, P. Y., Zhou, L., Porter, R., Cepada, A., Campirano, E., Licon, D., Lawrence, R., & Torres, M. (2020). Economic and technical assessment of rooftop solar photovoltaic potential in Brownsville, Texas, U.S.A. *Computers, Environment and Urban Systems, 80*, Article 101450.

Masson, V., Bonhomme, M., Salagnac, J. L., Briottet, X., & Lemonsu, A. (2014). Solar panels reduce both global warming and urban heat island. *Frontiers in Environmental Science, 2*(14), 1–10.

Meyers, S., Schmitt, B., & Vajen, K. (2018). Renewable process heat from solar thermal and photovoltaics: The development and application of a universal methodology to determine the more economical technology. *Applied Energy, 212*, 1537–1552.

Molina, A., Falvey, M., & Rondanelli, R. (2017). A solar radiation database for Chile. *Scientific Reports, 7*, 14823.

City of New York (2018). *Municipal solar-readiness assessment*. Accessed 30 June 2021 https://www1.nyc.gov/assets/dcas/downloads/pdf/energy/reportsandpublication/LL24_Solar_Readiness_Assessment_Report_2018.pdf.

NYC Open Data (2016). *Energy consumption – 2016 NYC*. Accessed 30 June 2021 https://data.cityofnewyork.us/Environment/Energy-Consumption-2016-NYC/85vh-khua.

NYC Open Data (2021a). *Energy and water data disclosure for local law 84 2020 (Data for calendar year 2019)*. Accessed 30 June 2021 https://data.cityofnewyork.us/Environment/Energy-and-Water-Data-Disclosure-for-Local-Law-84-/wcm8-aq5w.

NYC Open Data (2021b). *Electric consumption and cost (2010 – April 2020)*. Accessed 30 June 2021 https://data.cityofnewyork.us/Housing-Development/Electric-Consumption-And-Cost-2010-April-2020-/jr24-e7cr.

NYC Open Data (2021c). *Shapefile of footprint outlines of buildings in New York City*. Accessed 30 June 2021 https://data.cityofnewyork.us/Housing-Development/Building-Footprints/nqwf-w8eh.

Nyholm, E., Odenberger, M., & Johnsson, F. (2017). An economic assessment of distributed solar PV generation in Sweden from a consumer perspective e The impact of demand response. *Renewable Energy, 108*, 169–178.

Oberbeck, L., Alvino, K., Goraya, B., & Jubault, M. (2020). IPVF's PV technology vision for 2030. *Progress in Photovoltaics, 28*(11), 1207–1214.

Oh, J., Koo, C., Hong, T., & Cha, S. H. (2018). An integrated model for estimating the techno-economic performance of the distributed solar generation system on building façades: Focused on energy demand and supply. *Applied Energy, 228*, 1071–1090.

Park, A., & Lappas, P. (2017). Evaluating demand charge reduction for commercial-scale solar PV coupled with battery storage. *Renewable Energy, 108*, 523–532.

Peronato, G., Rey, E., & Andersen, M. (2018). 3D model discretization in assessing urban solar potential: the effect of grid spacing on predicted solar irradiation. *Solar Energy, 176*, 334–349.

Poruschi, L., & Ambrey, C. L. (2019). Energy justice, the built environment, and solar photovoltaic (PV) energy transitions in urban Australia: A dynamic panel data analysis. *Energy Research & Social Science, 48*, 22–32.

Rauf, H., Gull, M. S., & Arshad, N. (2020). Complementing hydroelectric power with floating solar PV for daytime peak electricity demand. *Renewable Energy, 162*, 1227–1242.

Redweik, P., Catita, C., & Brito, M. (2013). Solar energy potential on roofs and facades in an urban landscape. *Solar Energy, 97*, 332–341.

Ren, M., Mitchell, C. R., & Mo, W. (2020). Dynamic life cycle economic and environmental assessment of residential solar photovoltaic systems. *Science of the Total Environment, 722*, Article 137932.

Renken, V., Sorg, M., Marschner, V., Gerdes, L., Gerdes, G., & Fischer, A. (2018). Geographical comparison between wind power, solar power and demand for the German regions and data filling concepts. *Renewable Energy, 126*, 475–484.

Richardson, D. B., & Harvey, L. D. D. (2015). Strategies for correlating solar PV array production with electricity demand. *Renewable Energy, 76*, 432–440.

Staffell, I., & Pfenninger, S. (2018). The increasing impact of weather on electricity supply and demand. *Energy, 145*, 65–78.

Sun Earth Tools (2021). Tools for consumers and designers of solar. Accessed 30 June 2021 https://www.sunearthtools.com/dp/tools/pos_sun.php?lang=en.

Thanh, T. N., Minh, P. V., Trung, K. D., & Anh, T. D. (2021). Study on performance of rooftop solar power generation combined with battery storage at office building in Northeast Region, Vietnam. *Sustainability, 13*, 11093.

Tomar, V., & Tiwari, G. N. (2017). Techno-economic evaluation of grid connected PV system for households with feed in tariff and time of day tariff regulation in New Delhi – A sustainable approach. *Renewable and Sustainable Energy Reviews, 70*, 822–835.

Ullah, H., Kamal, I., Ali, A., & Arshad, N. (2018). Investor focused placement and sizing of photovoltaic grid-connected systems in Pakistan. *Renewable Energy, 121*, 460–473.

Wolske, K. S., Toddc, A., Rossol, M., McCalld, J., & Sigrin, B. (2018). Accelerating demand for residential solar photovoltaics: Can simple framing strategies increase consumer interest? *Global Environmental Change, 53*, 68–77.

Wong, M. S., Zhu, R., Kwok, Y. T., Kwan, M. P., Santi, P., Lee, K. H., Heo, J., Li, H., & Ratti, C. (2021). Association between NO$_2$ concentrations and spatial configuration: A study of the impacts of COVID-19 lockdowns in 54 US cities. *Environmental Research Letters, 16*, Article 054064.

Wong, M. S., Zhu, R., Liu, Z., Lu, L., Peng, J., Tang, Z., Lo, C. H., & Chan, W. K. (2016). Estimation of Hong Kong's solar energy potential using GIS and remote sensing technologies. *Renewable Energy, 99*, 325–335.

World Weather Online (2021). Historical monthly weather. Accessed 30 June 2021 https://www.worldweatheronline.com.

Zhang, J., Xua, L., Shabunko, V., Tay, S. E. R., Sun, H., Lau, S. S. Y., & Reindl, T. (2019). Impact of urban block typology on building solar potential and energy use efficiency in tropical high-density city. *Applied Energy, 240*, 513–533.

Zhong, T., Zhang, K., Chen, M., Wang, Y., Zhu, R., Zhang, Z., Zhou, Z., Qian, Z., Lv, G., & Yan, J. (2021). Assessment of solar photovoltaic potentials on urban noise barriers using street-view imagery. *Renewable Energy, 168*, 181–194.

Zhong, T., Zhang, Z., Chen, M., Zhang, K., Zhou, Z., Zhu, R., Wang, Y., Lv, G., & Yan, J. (2021). A city-scale estimation of rooftop solar photovoltaic potential based on deep learning. *Applied Energy, 298*, Article 117132.

Zhou, Y., Chen, M., Tang, Z., & Mei, Z. (2021). Urbanization, land use change, and carbon emissions: Quantitative assessments for city-level carbon emissions in Beijing-Tianjin-Hebei region. *Sustainable Cities and Society, 66*, Article 102701.

Zhu, R., Guilbert, E., & Wong, M. S. (2017). Object-oriented tracking of the dynamic behavior of urban heat islands. *International Journal of Geographical Information Science, 31*(2), 405–424.

Zhu, R., Guilbert, E., & Wong, M. S. (2020). Object-oriented tracking of spatial and thematic dynamic behaviors of urban heat islands. *Transactions in GIS, 24*, 85–103.

Zhu, R., Wong, M. S., Guilbert, E., & Chan, P. W. (2017). Understanding heat patterns produced by vehicular flows in urban areas. *Scientific Reports, 7*, 16309.

Zhu, R., Wong, M. S., You, L., Santi, P., Nichol, J., Ho, H. C., Lu, L., & Ratti, C. (2020). The effect of urban morphology on the solar capacity of three-dimensional cities. *Renewable Energy, 153*, 1111–1126.

Zhu, R., You, L., Santi, P., Wong, W. S., & Ratti, C. (2019). Solar accessibility in developing cities: A case study in Kowloon East, Hong Kong. *Sustainable Cities and Society, 51*, Article 101738.